High-Resolution Photothermal Laser Probe

CLAYTON C. WILLIAMS, MEMBER, IEEE

Abstract—**An advance in photothermal imaging is described. A photothermal laser probe is presented that operates at a frequency of 1 GHz. At this frequency the spacial resolution is limited only by the optical spot size of the probe beam. The photothermal sensitivity of the probe is 1.2×10^{-4} degrees celsius with a 5-mW probe beam and a 1-Hz bandwidth. The theoretical basis for the photothermal sensitivity will be presented along with an experimental description and verification of the theory. High-resolution photothermal images of implanted silicon will also be presented.**

I. Introduction

MOST PHOTOTHERMAL and photoacoustic imaging techniques have limited sensitivities at frequencies where the thermal wavelength is smaller than the region over which periodic heat can be deposited. Under these circumstances, the photothermal resolution is limited by the frequency of operation. This paper describes a photothermal laser probe that operates near 1 GHz. At this frequency the thermal wavelength in solids is small compared to the wavelength of light, and the resolution is essentially limited only by optical diffraction. The photothermal probe is a noncontacting optical technique that is based on photoelastic coupling between optical and acoustical fields in a high-pressure gas under collinear Bragg-scattering conditions.

The photothermal probe has been implemented in the following arrangement. An intensity modulated pump beam is tightly focused onto the surface of a solid in a cell filled with argon gas at high pressure (see Fig. 1). The modulated pump beam generates a harmonic temperature distribution that couples to an acoustic wave in the gas at the surface of the solid. A second beam, the probe, is collinearly aligned with the pump and also tightly focused to the same location on the sample. When the modulation frequency of the pump beam is near 1 GHz, the collinear Bragg-scattering condition is met, and a portion of the probe beam is back-scattered or back-reflected from the sound propagating in the gas. The probe light, which is scattered from the sound in the gas, is shifted upwards in frequency, so it can be heterodyned in an optical detector with the probe light, which is reflected from the solid surface (see Fig. 2). As will be explained in later sections, the heterodyne signal is proportional to the ac surface temperature over the region of the solid that is illuminated by the tightly focused probe beam. A photothermal image is obtained by scanning the object in two dimensions relative to the focused beams. This provides a measure of the thermal properties of the solid with high spatial resolution.

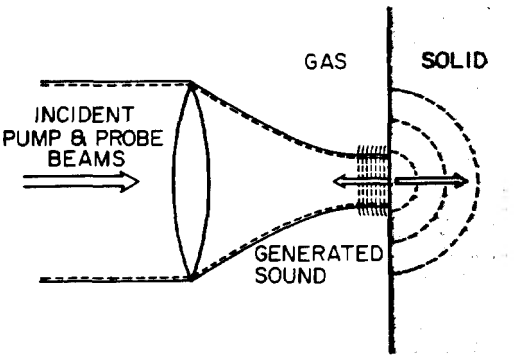

Fig. 1. Geometry of the photothermal laser probe.

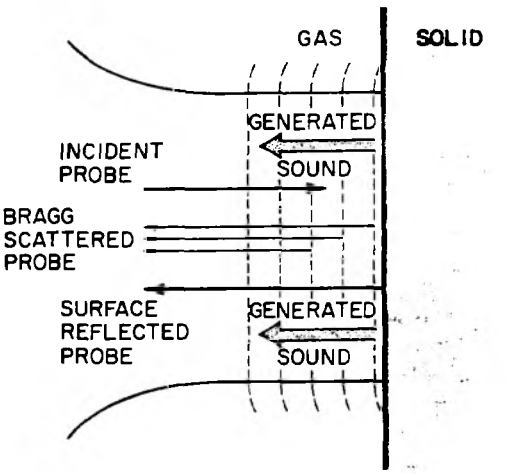

Fig. 2. Illustration of the two reflected components of the incident probe beam.

In this paper the theoretical basis for the photothermal laser probe will be presented. The sensitivity will be calculated with argon gas as the coupling medium. A figure of merit will also be established by which various coupling media may be evaluated. A comparison will then be made between three high resolution photothermal and photoacoustic techniques. Finally, an experimental description and verification of the theory will be presented including high-resolution photothermal images of boron-implanted silicon.

Manuscript received October 16, 1984; revised November 5, 1984. This work was supported by the Air Force Office of Scientific Research.

The author was with the Edward L. Ginzton Laboratory, Stanford University, Stanford, CA 94305. He is now with the IBM T. J. Watson Research Center, Yorktown Heights, NY 10598, USA.

0018-9537/85/0300-0365$01.00 © 1985 IEEE

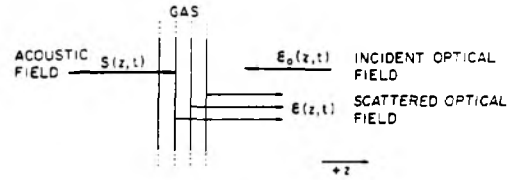

Fig. 3. Collinear Bragg-scattering geometry.

II. Acoustic Bragg-Scattering Efficiency

When optical and acoustic fields are superimposed in a solid, liquid, or gas, a nonlinear optical polarization is generated at the sum and difference frequency of the two driving fields. The nonlinear polarization reradiates or scatters the incident fields with an efficiency that depends upon the coherent summation of the nonlinear source over the interaction region. In this section the acoustooptic scattering efficiency in a gas will be calculated under one-dimensional collinear Bragg-scattering conditions (see Fig. 3).

The justification for using a one-dimensional analysis to treat the acoustooptic scattering of a focused optical probe beam by a focused acoustic beam is the following. Because the acoustic attenuation of the gas is extremely high, the interaction region of the optical and acoustic beams is very short, on the order of several micrometers. Over this distance the wavefronts of the acoustic and optical beams at focus remain quite well matched, even under fairly tight focusing conditions. When the wavefronts are matched, and all the scattered light can be collected within the angular aperature of the collection objective, a one-dimensional analysis should adequately predict the scattering efficiency of the acoustooptic interaction.

A. Inhomogeneous Wave Equation with Acoustooptic Source Term

Beginning with Maxwell's equations and the constitutive relations for an isotropic lossless medium, one obtains the familiar one-dimensional traveling wave equation with a nonlinear source polarization term [1]

$$\frac{\partial^2 \boldsymbol{E}}{\partial z^2} + \frac{\boldsymbol{n}^2 \partial \boldsymbol{E}}{c^2 \partial t^2} = -\mu \frac{\partial^2 \boldsymbol{P}^{NL}}{\partial t^2} \tag{1}$$

where $\boldsymbol{E}$ is the scattered electric field strength as a function of time and space; n is the index of refraction at the frequency of interest; c is the velocity of light in vacuum; μ is the permeability; and $\boldsymbol{P}^{NL}$ is the acoustooptic nonlinear polarization, also a function of time and space. The scattered electric field component $\boldsymbol{E}$ and nonlinear source polarization $\boldsymbol{P}^{NL}$ are defined to be of the following form:

$$\boldsymbol{E} = \boldsymbol{E}(z, t) = \mathrm{Re}\{E e^{j(wt - z)}\} \tag{2}$$

$$\boldsymbol{P}^{NL} = \boldsymbol{P}^{NL}(z, t) = \mathrm{Re}\{P^{NL} e^{j(wt - kz)}\} \tag{3}$$

where E and P^{NL} are envelope functions of $\boldsymbol{E}$ and $\boldsymbol{P}^{NL}$. Both are functions of time and space. If these definitions are substituted into (1), and the slowly varying envelope approximation is employed in steady state, the result is

$$\left(\frac{\partial E}{\partial z} = -j \frac{1}{2} \omega \eta P^{NL}\right) \tag{4}$$

where $\eta = \sqrt{(\mu/\epsilon)}$ is the wave impedance of the medium. Integration over the source region results in the following:

$$E = \int_0^z -\tfrac{1}{2} \omega \eta P^{NL}(z', t)\, dz' + E(0). \tag{5}$$

This equation relates the scattered electric field strength E to the nonlinear polarization envelope function P^{NL}.

B. Calculation of the Acoustooptic Nonlinear Source Polarization

Before calculating the nonlinear source polarization term, the photoelastic relation in the gas must be established. It can be obtained using the Lorentz–Lorenz formula [2]

$$\alpha_{\mathrm{pol}} = \frac{3\epsilon_0(\epsilon - 1)}{N(\epsilon + 2)} \tag{6}$$

where α_{pol} is the mean polarizability of the atoms or molecules; ϵ_0 is the permittivity of the free space; ϵ is the relative dielectric constant; and N is the number of atoms or molecules per unit volume. For a gas, where $(\epsilon - 1)$ is much less than one, it can be shown that

$$(\epsilon - 1) \approx \frac{N\alpha_{\mathrm{pol}}\rho}{\mathrm{MW}\epsilon_0}, \tag{7}$$

where MW is the molecular or atomic weight of the medium, and ρ is the density. The derivative of (7) provides a relation between a change in density of the gas $\delta\rho$, and the corresponding change in the relative dielectric constant $\delta\epsilon$. The result is

$$\delta\epsilon = (\epsilon - 1)\frac{\delta\rho}{\rho_0} = (\epsilon - 1)S \tag{8}$$

where

$$S = \frac{\rho - \rho_0}{\rho_0} \tag{9}$$

is the acoustic condensation. Equation (8) is the photoelastic relation for an ideal gas.

The nonlinear polarization $\boldsymbol{P}^{NL}$ can now be calculated using the constitutive and photoelastic relations in the gas, and the two incident optical and acoustic fields. The constitutive relation in the gas is given by

$$\boldsymbol{P} = \epsilon_0 \epsilon \mathbf{E}. \tag{10}$$

The change in polarization $\delta\boldsymbol{P}$ caused by a change in the dielectric constant $\delta\epsilon$, given an electric field E, is

$$\delta\boldsymbol{P} = \epsilon_0 \delta\epsilon \boldsymbol{E}. \tag{11}$$

Combining (8) and (11) the nonlinear polarization is given by

$$\boldsymbol{P}^{NL} = \delta\boldsymbol{P} = \epsilon_0(\epsilon - 1)S\boldsymbol{E}. \tag{12}$$

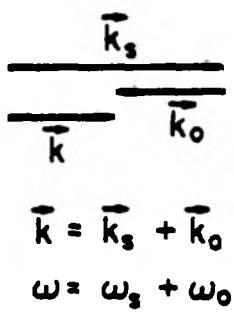

Fig. 4. The k-vector matching condition for collinear Bragg-scattering.

The nonlinear polarization can be seen to be proportional to the product of the incident acoustic and optical field strengths.

C. Scattering Efficiency

The nonlinear polarization envelope can now be substituted into (5) to provide a relationship between the scattered electric field and the incident optical and acoustic fields under collinear scattering conditions. If the k-vector mismatch (see Fig. 4) is defined as

$$\Delta k = k_0 - k_s + k \tag{13}$$

and the scattering is assumed to be weak, with the exponential sound attenuation constant α, and no contribution to the scattered field for z less than zero

$$E_0(z) \approx E_0 \tag{14}$$

$$S(z) = S_0 e^{-\alpha z} \tag{15}$$

$$E(0) = 0 \tag{16}$$

The scattered electric field strength is given by

$$E(z, t) = -j \frac{1}{4} \omega \eta \epsilon_o (\epsilon - 1) S_0 E_0 e^{j(\omega o + \omega_s - \omega)t} \cdot \int_0^z e^{-\alpha z'} e^{j\Delta k z'} dz'. \tag{17}$$

If the k-vector matched case is assumed, $\Delta k = 0$, the ratio of the scattered power to the incident optical power is given by

$$\Gamma = \left|\frac{E}{E_0}\right|^2 = \left[\frac{(\epsilon - 1) S_0}{2\alpha\lambda_0}\right]^2 \tag{18}$$

where Γ is the acoustic Bragg-scattering efficiency, and λ_0 is the vacuum wavelength of the probe beam. If no assumption is made about the k-vector matching, (17) must be evaluated for a nonzero Δk. If the integral is evaluated at a position z, far from the interaction region ($z \gg 1/\alpha$), the upper limit of the integral can be replaced by infinity without effecting the result. The scattering efficiency in this case becomes

$$\Gamma = \left[\frac{(\epsilon - 1) S_0}{2\alpha\lambda_0}\right]^2 \frac{1}{\left(1 + \left(\frac{\Delta k}{\alpha}\right)^2\right)}, \tag{19}$$

where $\Delta k = (\omega - \omega_0)/V_a$ and ω_0 is the acoustic frequency for which Δk is zero. Equation (19) provides a relation between the Bragg-scattering efficiency Γ and the peak acoustic condensation S_0 in the gas under collinear scattering conditions for arbitrary k-vector mismatch. It predicts that the scattering efficiency has a Lorenzian dependence upon the frequency of the acoustic wave in the gas.

III. Heterodyne Sensitivity

Since the Bragg-scattered light is upshifted in frequency, detection is made possible by optically mixing it in a photodetector with the unshifted light reflected from the surface of the solid. The optical mixing provides a very sensitive means of measuring the amount of Bragg-scattered light. The sensitivity is large because the heterodyne signal is proportional to the product of the signal (shifted) and reference fields (unshifted). When the reference field is large compared to the signal field, the heterodyne sensitivity can be many orders of magnitude better than direct detection of the scattered light. Furthermore, the signal can be optically mixed to a frequency where there is essentially no interference or background. To calculate the sensitivity of the probe, the noise contributed in the detection and amplification process must be taken into account. In this section the signal-to-noise ratio of the probe will be calculated as a function of the Bragg-scattering efficiency.

The sensitivity of the heterodyne detection will be evaluated under the following conditions. The incident probe beam of average power P_0 is reflected by the sound in the gas with power reflection coefficient Γ and reflected from the sample surface with power reflection coefficient R. Both reflected components propagate collinearly back to the photodetector, where they generate a heterodyne signal at the frequency of the acoustic wave in the gas. The optical heterodyne power is proportional to the product of the fields from these two reflections. The peak optical heterodyne power at the acoustic frequency (w_a) is given by

$$P_{\text{het}} = 2\sqrt{RP_0}\,\sqrt{\Gamma P_0} = 2\sqrt{R}\,\sqrt{\Gamma} P_0. \tag{20}$$

Conversion of the optical heterodyne power to an RF signal takes place in the photodetector. The peak heterodyne current is given by

$$I_{\text{het}} = \alpha_r P_{\text{het}} \tag{21}$$

where α_r is the responsivity (amps/watt) of the photodetector. The average signal power into the load resistor is thus given by

$$P_{\text{signal}} = \tfrac{1}{2} I_{\text{het}}^2 R_l = 2\alpha_r^2 R\Gamma P_0^2 R_l. \tag{22}$$

There are three sources which contribute noise to the signal as it is detected and amplified: shot noise, Johnson noise, and amplifier noise. The total noise power contributed by these three sources is given by [3], [4]

$$P_{\text{noise}} = 4KTBF + 2e\alpha_r BRP_0 R_l \tag{23}$$

where K is the Boltzmann's constant; T is the absolute

temperature; B is the bandwidth; F is the noise figure of the preamplifier; e is the electron charge; α_r is the detector responsivity (A/W); R_l is the load resistance; and P_0 is the average detected power. Thus the signal-to-noise ratio is given by

$$\frac{S}{N} = \frac{2\alpha_r^2 R\Gamma P_0^2 R_l}{4KTBF + 2e\alpha_r BRP_0 R_l}. \tag{24}$$

This equation establishes the relationship between the signal-to-noise ratio and the Bragg-scattering efficiency Γ, given the other detection system parameters.

One interesting point about the Bragg interaction must be made. After the incident probe beam is reflected from the surface of the solid, it sees another traveling acoustic wave. The Bragg condition is met once again for back scattering. However, the frequency in this case is down-shifted because the sound wave is receding from the solid. The down-shifted light propagates back to the solid, where it is reflected, and then propagates away with the upshifted light. The result is a double sidebanded carrier. The phase relation between the upper and lower sideband relative to the carrier is identical to that found when phase modulation takes place. The distinguishing feature, however, is that the lower sideband has gone through two reflections from the surface of the solid. Since the reflectivity of the solid will always be less than one, the amplitude of the lower sideband will always be less than the upper sideband by a factor of R, the power reflectivity of the solid. The heterodyne signal, with this effect included, is now proportional to the difference between the sideband amplitudes rather than the amplitude of the single sideband. To include this effect in the signal to noise ratio calculation, the reflectivity R in the numerator of (24) must be replaced by the following expression:

$$R(1 - R)^2. \tag{25}$$

One of the attractive features of this heterodyne scheme is that an interferometer is not required to detect the signal. This is the result of the fact that the sidebands on the carrier do not have equal amplitudes. In contrast, techniques that rely on phase modulation of an optical carrier, such as displacement interferometry, must use a reference local oscillator that is in quadrature with the center carrier for demodulation. These techniques generally require a stabilized interferometer.

There may be circumstances where the use of an interferometer arrangement with the Bragg detection may be desirable. In cases where the surfaces are rough or highly absorbing, there would be advantage to using a reference that does not depend upon the surface reflectivity of the material being imaged. In these cases the probe beam could be split, a portion sent into the cell to be Bragg-scattered by the sound propagating in the gas, and the rest sent to the reference arm of the interferometer. The reflection from the sound propagating in the gas could then be mixed with the reference beam and a signal obtained independent of the reflectivity of the solid. Under these circumstances, the signal-to-noise ratio would be given by (24) without the dependence upon the sample reflectivity. In most cases, however, the disadvantages of using a stabilized interferometer outweigh the problems of having a signal that is dependent upon the reflectivity of the sample surface.

IV. Thermoacoustic Generation of Sound

When the surface temperature of a solid varies harmonically with time, a periodic temperature distribution is generated in the surrounding gas. This temperature distribution couples to an acoustic wave through the expansion of the gas. If the amount of sound generated by the expansion of the gas is large compared to the sound generated by the thermally generated displacement of the solid, then a measurement of the sound in the gas is equivalent to a measure of the ac surface temperature of the solid.

A simple one-dimensional analysis can be used to determine under what conditions the contribution of the gas will be large compared to the contribution of the solid. The surface displacement of a solid when periodically heated at its surface can be shown to be approximately equal to [5]

$$U_s = \alpha_s \theta_0 \lambda_{ts} \tag{26}$$

where α_s is the linear coefficient of expansion of the solid; θ_0 is the peak sinusoidal temperature variation at the surface of the solid; and $\lambda_{ts} = \sqrt{(2\kappa_s/\omega)}$ is the thermal wavelength in the solid. This surface displacement U_s causes an equal displacement in the gas, since the acoustic displacement at the interface must be continuous. In addition, the thermal expansion of the gas generates a displacement in the gas, which is given by

$$U_g = \alpha_g \theta_0 \lambda_{tg} \tag{27}$$

where the same definitions as above apply for the gas. Since the acoustic power density is proportional to the square of the displacement, the ratio squared of the two displacements gives the relative amount of power contributed by the expansion of gas as compared with the expansion of the solid

$$\frac{P_g}{P_s} = \left|\frac{U_g}{U_s}\right|^2 = \frac{\alpha_g^2 \kappa_g}{\alpha_s^2 \kappa_s}. \tag{28}$$

Table I shows the relative power contribution of argon gas at a pressure of 100 atmospheres as compared with several solids. As can be seen from the table, for many materials, the amount of acoustic power in the gas is essentially determined only by the temperature fluctuation at the surface of the solid.

When the optical absorption depth L_{opt} is finite, the calculation shown above must be modified. Under this condition, the displacement ratio is approximated by the following expression.

$$\frac{U_g}{U_s} = \frac{\alpha_g \lambda_{tg}}{\alpha_s(\lambda_{ts} + L_{\text{opt}})}. \tag{29}$$

TABLE I
RELATIVE SOURCE STRENGTH OF ACOUSTIC POWER IN THE GAS [6], [7]

	Silicon	Fused Quartz	Gold	Aluminum
Exp. Coeff. (α_s)	2.5×10^{-6}	5.5×10^{-7}	1.3×10^{-5}	2.3×10^{-5}
Diffusivity (κ)	1.0×10^{-4}	8.3×10^{-7}	1.3×10^{-4}	9.6×10^{-4}
Power ratio (P_g/P_s)	4.3×10^{2}	1.1×10^{6}	1.2×10^{1}	5.33

In silicon, where the optical absorption depth is approximately 4000 Å for green light, the power contributed by the gas is nearly two orders of magnitude larger than that contributed by the solid.

Since the acoustic power in the gas is essentially determined by the harmonic temperature at the surface of the solid, a relationship can be established between this temperature and the acoustic condensation in the gas. Because the acoustic impedance of the solid is much larger than that of the gas, the thermoacoustic generation of sound in the gas can be considered to be under contrained boundary conditions. The acoustic condensation generated thermoacoustically in the gas can be shown to be [5]

$$S_0 = \frac{k_a \alpha_g \theta_0}{k_t} \tag{30}$$

where k_a and k_t are the acoustic and thermal k-vectors in the gas; α_g is the expansion coefficient of the gas; and θ_0 is the peak ac temperature rise at the surface of the solid. This provides a relationship between the magnitude of the sinusoidal surface temperature of the solid θ_0 and the magnitude of the acoustic condensation in the gas S_0. This result can now be used to relate the Bragg-scattering efficiency to the harmonic surface temperature of the solid.

V. PHOTOTHERMAL SENSITIVITY

Using the results from the three previous sections, the photothermal sensitivity of the probe can be calculated. Combining (18) from Section II and (30) from the previous section, the Bragg-scattering efficiency Γ under phase matched conditions can be related to the harmonic surface temperature θ_0

$$\Gamma = \left[\frac{\pi(\epsilon - 1)S_0}{2\alpha\lambda_0}\right]^2 = \left[\frac{\pi(\epsilon - 1)}{2\alpha\lambda_0}\right]^2 \left(\frac{k_a \alpha_g}{k_t}\right)^2 \theta_0^2. \tag{31}$$

If this relation is substituted into equation (24) of Section III

$$\frac{S}{N} = \frac{2\alpha_r^2 R \Gamma P_0^2 R_l}{4KTBF + 2e\alpha_r BRP_0 R_l} \tag{32}$$

an expression is obtained for the signal-to-noise ratio as a function of the harmonic surface temperature of the solid

$$\frac{S}{N} = \left(\frac{2\alpha_r^2 R P_0^2 R_l}{4KTBF + 2e\alpha_r BRP_0 R_l}\right) \cdot \left[\frac{\pi(\epsilon - 1)}{2\alpha\lambda_0}\right]^2 \left(\frac{k_a \alpha_g}{k_t}\right)^2 \theta_0^2. \tag{33}$$

TABLE II
EXPERIMENTAL CONDITIONS—ARGON GAS (100 atm., 300°K)

Detector responsivity	α_r	.33 A/W
Sample reflectance	R	.5
Incident optical power	P_0	5.0 mW
Load resistor	R_l	50 Ω
Boltzman constant	K	1.38×10^{-23} J/°K
Temperature	T	300°K
Noise figure	F	1.77 (2.5 db)
Optical wavelength	λ_0	632 nm
Dielectric constant	ϵ	1.055
Acoustic atten. const.	α	1.7×10^5/m
Acoustic k-vector (1.03 GHz)	k_a	1.98×10^7/m
Linear expansion coeff.	α_g	1.11×10^{-3}
Thermal k-vector (1.03 GHz)	k_t	1.2×10^8/m

This characterizes the photothermal sensitivity of the probe. Table II contains the experimental conditions under which this sensitivity will be evaluated. With these values, the photothermal sensitivity is given by

$$\frac{S}{N} = \left(\frac{6.9 \times 10^7}{B}\right)\theta_0^2. \tag{34}$$

In a 1-Hz bandwidth, the minimum detectable harmonic temperature variation is given by

$$\theta_{\min} = 1.2 \times 10^{-4}\,°\text{C} \tag{35}$$

This sensitivity compares very favorably with the sensitivities of other techniques as shown in Section VII. Furthermore, this temperature variation need not occur over a region larger than the optical probe spot size.

VI. ACOUSTOOPTIC COUPLING MEDIUM—FIGURE OF MERIT

In the previous section a relation was established between the signal-to-noise ratio and the ac temperature at the solid surface given the optical, electrical, and physical properties of the detection system. This relation was then used to calculate the photothermal sensitivity with argon gas as the acoustooptic coupling medium. Although argon gas is very attractive as an acoustooptic coupler, many other gases and liquids could potentially be used to couple the photothermally generated sound to the probe beam. In this section a figure of merit for the coupling medium will be derived from (33) of the previous section, and various liquids and gases will then be evaluated for use in the photothermal laser probe.

The sensitivity of the photothermal probe depends upon the characteristics of the acoustooptic coupling medium through the following parameters: the dielectric constant

TABLE III
ACOUSTOOPTIC COUPLING MEDIA

Media	Bragg Frequency (GHz)	Figure of Merit
Argon gas (100 atm.)	1.03	1.0
Argon liquid (87°K)	2.7	360
Nitrogen liquid (77°K)	2.7	4.7
Helium liquid (4.2°K)	0.57	150
Water (300°K)	4.9	0.12
Air (300°K, 1 atm.)	1.0	10^{-6}

ϵ; acoustic attenuation constant α; acoustic velocity V_a; linear expansion coefficient α_g; and thermal diffusivity κ. A figure of merit can be defined using these parameters in such a way as to make possible the relative evaluation of different acoustooptic coupling media. The signal-to-noise ratio calculated in the previous section is proportional to the properties of the coupling medium in the following way

$$\frac{S}{N} \propto \frac{(\epsilon - 1)^2 \alpha_g^2 \kappa}{\left(\frac{\alpha}{f^2}\right)^2 V_a^3}. \tag{36}$$

A figure of merit is obtained if the right side of this equation is normalized by the signal-to-noise ratio obtained with a reference medium: argon gas at a pressure of 100 atmospheres

$$F.M. = (8.9 \times 10^6) \frac{(\epsilon - 1)^2 \alpha_g^2 \kappa}{\left(\frac{\alpha}{f^2}\right)^2 V_a^3}. \tag{37}$$

Table III shows several different gases and liquids with their associated figure of merit as calculated using (37).

As can be seen, there are reasons for using cryogenic liquids as the coupling media. This may be especially interesting for evaluation crystaline defects and doping in silicon or other semiconductors. At room temperature, the thermal conductivity of silicon is almost independent of the defect concentration unless the density is greater than $10^{18}/cm^3$ [8]. The reason for this is that the dominant phonon scattering mechanism at room temperature is three-phonon scattering or umklapp scattering. Only at lower temperatures is the scattering dominated by impurity scattering. Theory predicts that with liquid argon (87°K) as the coupling liquid, defect densities well below $10^{18}/cm^3$ should be measurable. Furthermore, the sensitivity of the probe is enhanced by more than two orders of magnitude by the use of liquid argon rather than the high-pressure gas. Working with liquid argon would also require that a higher pump beam modulation frequency be used as is shown in Table III.

VII. COMPARISON OF PHOTOACOUSTIC AND PHOTOTHERMAL TECHNIQUES

It is difficult to make a direct comparison of many of the available photothermal and photoacoustic techniques due to the wide range of applications, resolution requirements and frequencies employed. There are several high-resolution techniques, however, that can be evaluated and compared in a clear way when performing a specific function. The three techniques that will be compared are photodisplacement interferometry, photoacoustic detection with an acoustic lens, and photothermal Bragg detection. The comparison can be made by calculating for each technique the smallest harmonic temperature variation at the surface of a solid that can be detected within a given bandwidth. The evaluation will be made at a frequency of 1 GHz, since the photothermal Bragg detection is locked at this frequency by the Bragg resonance. After calculation of the individual sensitivities of these three techniques, the results will be discussed and compared.

To determine the sensitivity of photothermal displacement interferometry, a periodic temperature at the surface of a solid must be related to the thermoacoustically generated displacement. Then, using published values of displacement sensitivity, the sensitivity to periodic temperature can be calculated.

If a solid is periodically heated at its surface, the resultant harmonic temperature varies over a region of approximately one thermal wavelength. The resultant surface displacement is given approximately by [5]

$$U_s = \theta_0 \alpha_s \lambda_{ts} \tag{38}$$

where θ_0 is the peak harmonic temperature; α_s is the linear expansion coefficient; and λ_{ts} is the thermal wavelength at the frequency of the harmonic temperature. This provides the relation between harmonic temperature and surface displacement. The minimum detectable surface displacement with interferometry has been reported as 3×10^{-4} Å with a 0.1 second integration time [9]. The displacement sensitivity is therefore given by

$$U_{\min} = \frac{10^{-4}\ \text{Å}}{\sqrt{\text{Hz}}}. \tag{39}$$

The combination of the two previous relations provides a photothermal sensitivity for displacement interferometry, given by

$$\theta_{\min} = \frac{10^{-4}\ °\text{C}}{\alpha_s \lambda_{ts} \sqrt{\text{Hz}}}. \tag{40}$$

For the case of the acoustic lens, the surface displacement must be converted to an acoustic power density in the coupling liquid. The assumption is made that the acoustic loading of the surface displacement by the coupling liquid is small. This is a good approximation because the impedance of most liquids is very small compared to the impedance of solids. Without loading, the power density in the liquid created by the displacement of the solid is given by

$$\frac{P}{A} = \frac{1}{2} Z_l \omega^2 U_s^2 \tag{41}$$

where Z_l is the acoustic impedance of the liquid, and ω is

the radian frequency of the modulation. Using (38), this power density can be related to the surface temperature of the solid

$$\frac{P}{A} = \left(\frac{1}{2} Z_l \omega^2 \alpha_s^2 \lambda_{ts}^2 \theta_0^2\right). \tag{42}$$

The total acoustic power generated by this periodic temperature over a given area is

$$P = \left(\frac{P}{A}\right) (\text{area}). \tag{43}$$

The photothermal sensitivity for the acoustic lens can now be calculated. If the acoustic detection efficiency of the lens is near 10^{-2}—including attenuation at 1 GHz—and the noise is given by 10^{-20} W/Hz, the minimum detectable acoustic power at the focus is approximately given by

$$P_{\min} = \frac{10^{-18}}{\text{Hz}} \text{ watts}. \tag{44}$$

The photothermal sensitivity of the acoustic lens is therefore given by

$$\theta_{\min} = \sqrt{\frac{2P_{\min}}{Z_l \text{area}}} \left(\frac{1}{\omega \alpha_s \lambda_{ts}}\right) °\text{C}. \tag{45}$$

The expressions for the photothermal sensitivity of interferometry and acoustic lens techniques will now be evaluated using material values for silicon and one-square-micrometer area. Under these conditions, the minimum detectable harmonic temperature for the interferometric technique is give by

$$\theta_{\min} = \frac{2.2 \times 10^{-2} °\text{C}}{\sqrt{\text{Hz}}}. \tag{46}$$

The photothermal sensitivity of the acoustic lens is given by

$$\theta_{\min} = \frac{4.1 \times 10^{-4} °\text{C}}{\sqrt{\text{Hz}}}. \tag{47}$$

The sensitivity of Bragg detection was calculated in Section V. The result was

$$\theta_{\min} = \frac{1.2 \times 10^{-4} °\text{C}}{\sqrt{\text{Hz}}}. \tag{48}$$

Comparing these sensitivities, it is clear that for the case of silicon, the Bragg detection compares favorably with the other techniques. Because the photothermal sensitivity of the interferometric and acoustic lens techniques depend upon the expansion coefficient and thermal wavelength, the relative sensitivities will depend upon the material being examined. However, two points must be made. First, it can be shown that the acoustic lens technique will always remain more sensitive than the interferometry. Second, it can be shown that the 1-GHz photothermal sensitivity of Bragg detection will always be much greater than that of displacement interferometry if the pressure of the argon gas is greater than 120 atmospheres.

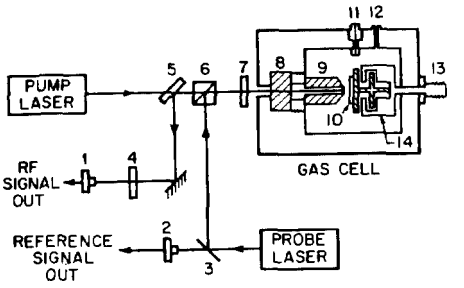

Fig. 5. Schematic diagram of the photothermal surface probe. (1), (2) fast silicon diodes; (3) beamsplitter; (4) spike interference filter; (5) dicroic mirror; (6) polarizing beamsplitter; (7) quarter-wave plate; (8) optical window; (9) focusing objective; (10) sample; (11) electrical feedthrough; (12) gas input; (13) focusing micrometer; (14) electromechanical scanner.

VIII. Experimental Verification of the Theory

A. Experimental Implementation

A schematic diagram of the photothermal surface probe is shown in Fig. 5. A pump laser, modulated at 1.03 GHz, is focused by an optical microscope objective inside the gas cell to a diffraction limited spot on the sample surface. The absorbed optical power photothermally generates sound, which propagates away from the solid.The probe laser is directed through a quarter-wave plate into the cell by a partial mirror and a polarizing beam splitter, where it is focused to the same location as the pump beam. There, it is reflected at the sample surface as well as by the sound wave propagating in the gas. These two reflected components are then recollimated by the optical objective and pass through the quarter wave plate a second time. The two passes through the quarter-wave plate cause a 90-degree rotation of the polarization. The reflected probe therefore propagates through the polarizing beam splitter. It is then reflected by a dicroic mirror and finally passes through a narrow-band interference filter to a fast photodiode. The interference filter isolates the photodiode from the pump laser power. The cell is pressurized to 50–100 atmospheres by simply connecting it through a high-pressure regulator to a standard argon gas cylinder. The sample is positioned at focus by a micrometer from outside the gas cell. An electromechanical scanner [10] inside the gas cell makes possible two-dimensional scanning of the sample with respect to the pump and probe beams. A reference signal at the frequency of the axial mode spacing of the probe laser (ω_r) is detected in a second photodetector.

To avoid the problems of RF interference that occur when detecting at the modulation frequency of the pump laser (ω_a), the two longitudinal modes of the He–Ne probe laser are used to optically mix the heterodyne signal to a frequency other than that of the acoustic wave. This is accomplished by optically mixing the Bragg shifted signal from one axial mode ($\omega_0 + \omega_a$) with the unshifted second axial mode ($\omega_0 + \omega_r$). The result is a heterodyne signal out of the optical detector at the difference between the

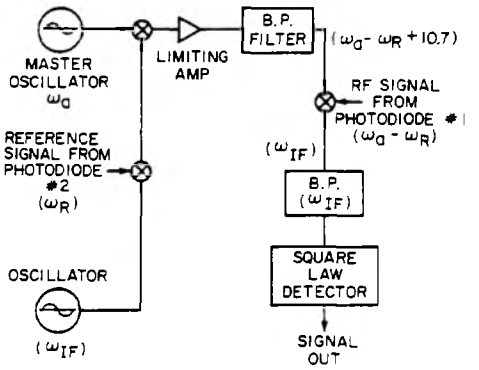

Fig. 6. Heterodyne detection system.

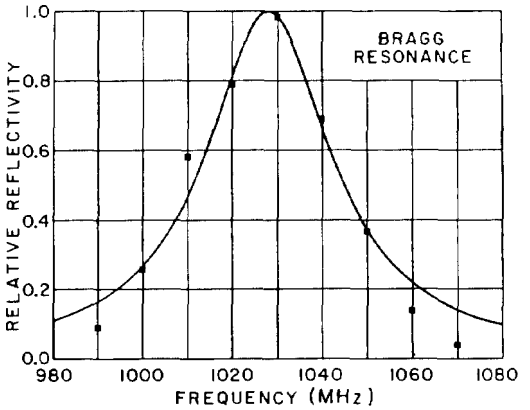

Fig. 7. Theoretically predicted collinear Bragg-scattering efficiency as a function of the frequency of sound in the gas and the experimental data.

acoustic frequency and the axial mode spacing ($\omega_a - \omega_r$). This signal is then mixed down to an IF frequency, filtered and square law detected (see Fig. 6). For phase sensitivity, the signal can also be mixed down to dc and detected with a lock-in amplifier.

B. Frequency Dependence

The frequency dependence of the Bragg interaction was measured in the following way. A small portion of the pump beam was split off, and the modulated optical power was monitored using a fast photodetector and an RF spectrum analyzer. While changing the modulation frequency of the pump, the signal from the probe beam was measured. The probe signal was then normalized by the modulated pump power as measured with the photodiode and spectrum analyzer. The experimental results are shown with the theoretically expected Lorentzian frequency dependence in Fig. 7.

C. Absolute Sensitivity

The absolute sensitivity of the probe to acoustic power was measured using a 1-GHz acoustic flat as the source of sound in the gas. The acoustic flat was chosen to measure the sensitivity for two reasons. First, the flat provides a fairly uniform acoustic power density over a relatively large area (10^4 μm^2). This makes the positioning of the probe beam a relatively simple task. The second reason is that it is possible to calculate the acoustic power density in a gas transmitted from the flat by measuring the RF input power and the insertion loss using a pulse echo technique. Measurement of the insertion loss of the transducer and calculation of the transmission of the sound from the flat into the gas determines the total acoustic power in the gas. The acoustic spot size can be calculated from the size of the transducer. This information provides a knowledge of the acoustic power density in the gas. To avoid any miscalculation due to a resonance of the flat itself, the insertion loss measurements were made using acoustic pulses that were shorter than the round-trip time in the flat.

To locate the region illuminated by the acoustic power on the front surface of the flat, the flat was illuminated by a focused modulated laser. The flat was scanned with respect to the laser spot, and an image was obtained of the photoacoustic sound detected by the flat in the receiving mode. A scanned optical reflection image was also obtained of the same region. Comparison of the two images identified the region where the acoustic illumination was to be found. The acoustic spot diameter was approximately 100 μm. The optical image was then used to locate this region for positioning the probe beam. The following are the experimental conditions and the minimum detectable acoustic intensity I_{min} in the gas:

$$P_{gas} = 50 \text{ atmospheres}$$

$$P_0 = 1.75 \text{ mW}$$

$$R_{eff} = .04$$

$$F = 1.77$$

$$B = 5 \text{ MHz}$$

$$R_l = 50\ \Omega$$

$$I_{min} = 5.5 \times 10^4 \text{ W/m}^2.$$

A calculation of the theoretical sensitivity to acoustic power in the gas using these experimental values indicates that the experimental sensitivity is a factor of 3.5 less than that predicted by theory. This value is not much larger than the combined experimental uncertainty in the measurement.

D. Dependence on Pressure

Using the same experimental arrangement described in the previous section, the pressure of the gas was varied as the measurement was made. The results showed that the signal was proportional to the pressure to a power of 2.5 over a range of 26 to 66 atmospheres. Thus

$$S \propto P_{gas}^{2.5}. \tag{49}$$

The theory predicts that the signal should vary as the third power of the pressure of the gas [11].

The most plausible explanation of the discrepancy between the theory and experiment is the following. Since the probe beam is highly focused and the sound delivered by the acoustic flat is essentially planar, the phase fronts of the two fields are most closely matched in the region

near the focus. Farther from the focus, the spherical phase curvature on the optical beam makes efficient heterodyning impossible due to the mismatch in the phase curvature between the scattered and reference beams. At low pressures, the acoustic attenuation is high, so the only region which contributes to the heterodyne signal is near the focus. As the pressure is increased, the regions farther from focus begin to contribute. However, due to the mismatch in the spatial phase fronts, they do not contribute as much as would be predicted by theory which assumes perfectly matched phase fronts. This could explain why the measured pressure dependence goes to a power of 2.5 rather than 3.0.

IX. Photothermal Imaging of Implanted Silicon

To demonstrate the sensitivity of the probe to variations in the thermal properties of materials, a silicon wafer was implanted with 150-keV boron through a resist pattern. After implantation, the patterned resist was plasma-etched, leaving only a thin oxide. This oxide was then removed, exposing a clean silicon surface. Thus, the silicon was left uniformly implanted, except in the regions where the resist had isolated the silicon from the boron implant. In these regions the silicon was intrinsic. The implant density was calculated to be $10^{18}/cm^3$ at the surface, increasing to $10^{21}/cm^3$ at a depth of 5000 Å.

The sample was imaged with the photothermal probe, and a variation in the thermal response of the implanted region (darker) relative to the unimplanted regions (lighter) was found. The photothermal image is shown in Fig. 8(a). The spacing of the *H*-like characters from center to center is approximately 15 microns. A three-percent variation in the optical reflection was measured from region to region due to the effects of the implantation. This optical variation is too small to account for the photothermal contrast seen in the image. However, to eliminate any optical variation, 300 Å of titanium were deposited on the silicon surface, and the sample was imaged again. Fig. 8(b) again shows the thermal contrast due to the boron implant. The titanium-covered silicon region (left) actually generates a larger photothermal signal than the silicon alone. This is largely due to the greater optical attenuation constant of the titanium. The signal from the uncoated silicon region (right) is not apparent in the image because the bias level and gain of the signal were adjusted to allow for maximum contrast in the titanium–silicon region. The source of contrast in the titanium-covered silicon region is the variation in the thermal wave reflectance at the interface between the titanium and silicon. These images clearly demonstrate the sensitivity of the probe to changes in the thermal properties of the silicon created by the boron implantation.

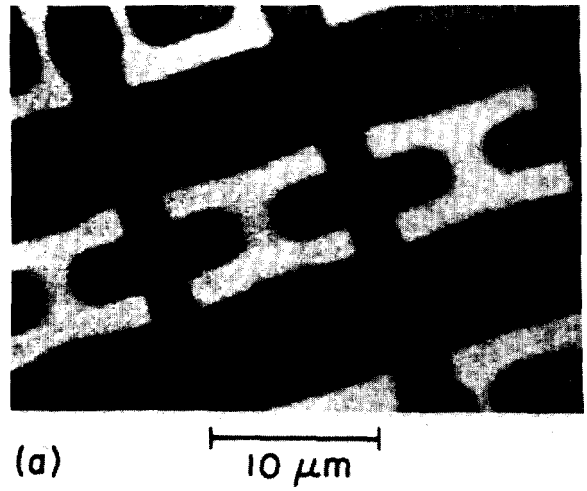

(a)

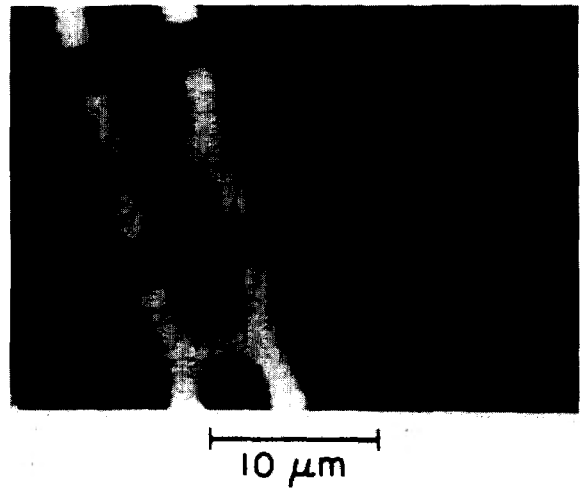

(b)

Fig. 8. Photothermal images of implanted silicon. The darker are is the implanted region, the lighter region is not implanted. (a) Boron-implanted silicon. (b) Implanted silicon with 300 Å of titanium deposited on the silicon in the left half of the image.

X. Summary

The theory behind the photothermal laser probe has been presented along with an experimental verification of the theory. The sensitivity has been shown to compare favorably with other high-resolution techniques. A figure of merit has been defined, and several coupling media have been evaluated. High-resolution images have been obtained, demonstrating the resolution and sensitivity of the probe to variations in the thermal properties of materials.

The features which distinguish this photothermal probe from other techniques are the high frequency of modulation, the noncontacting nature of the evaluation, and the high sensitivity to ac temperature variations over very small areas. In applications where the highest sensitivity and resolution is desired, the probe should provide a unique tool for materials evaluation.

Acknowledgment

The author would like to thank C. F. Quate for his support of this research. Also, thanks go to Larry Moberly, Jim Sturm, and John Foster for providing the silicon sample.

References

[1] Ammon Yariv, *Quantum Electronics*. New York: John Wiley, 1975, p. 356.

[2] M. Born and E. Wolf, *Principles of Optics*. Oxford: Pergamon, 1980, p. 87.

[3] R. L. Whitman and A. Korpel, "Probing of acoustic surface perturbations by coherent light," *Appl. Opt.*, vol. 8, p. 1567, 1969.

[4] R. M. De La Rue, R. F. Humphryes, I. M. Mason, and E. A. Ash, "Acoustic-surface-wave amplitude and phase measurements using laser probes," *Proc. Inst. Elec. Eng.*, vol. 119, p. 117, 1972.

[5] R. M. White, "Generation of elastic waves by transient surface heating," *J. Appl. Phys.* vol. 34, p. 3559, 1963.

[6] *AIP Handbook*, 3rd ed. Dwight E. Gray, Ed. New York: McGraw-Hill, 1972, pp. 4–142.

[7] *Handbook of Chemistry and Physics*, Robert C. Weast, Ed. Cleveland: CRC, 1975, p. F-78.

[8] S. Holland and R. M. White, "Concentration dependence of thermal-wave contrast for dopants in silicon," in *Proc. 1983 IEEE Ultrason. Symp.*, p. 681.

[9] J. E. Bowers, "Fiber-optic sensor for surface acoustic waves," *Appl. Phys. Lett.*, vol. 41, p. 231, 1982.

[10] J. Heiserman, D. Rugar, and C. F. Quate, "Cryogenic acoustic microscopy," *J. Acoust. Soc. Am.*, vol. 67, p. 1629, 1980.

[11] C. C. Williams, "High-resolution acoustooptic laser probe," in *Proc. 1983 IEEE Ultrason. Symp.*, p. 952.

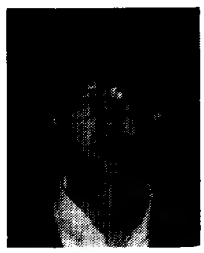

Clayton C. Williams (M–'84) was born in Salt Lake City, Utah on June 26, 1954. He received the B.A. degree in physics in 1979 from the University of Utah, Salt Lake City, UT, and the M.S. and Ph.D. degrees in electrical engineering from Stanford University, Stanford, CA, in 1981 and 1984, respectively.

At Stanford he worked in the area of high-frequency photoacoustic and photothermal imaging. After a postdoctoral appointment at Stanford, he joined IBM at the Thomas J. Watson Research Center, Yorktown Heights, NY, where he is currently working in the Measurement Technology Department of Manufacture Research. His current interests include noncontacting techniques for materials evaluation, profilometry, and metrology.